PHYSICAL REVIEW B **93**, 121110(R) (2016)

Optical spectroscopy of the Weyl semimetal TaAs

B. Xu,[1] Y. M. Dai,[2] L. X. Zhao,[1] K. Wang,[1] R. Yang,[1] W. Zhang,[1] J. Y. Liu,[1] H. Xiao,[1] G. F. Chen,[1,3] A. J. Taylor,[4] D. A. Yarotski,[2] R. P. Prasankumar,[2,*] and X. G. Qiu[1,3,†]

[1]*Beijing National Laboratory for Condensed Matter Physics, Institute of Physics, Chinese Academy of Sciences, P.O. Box 603, Beijing 100190, China*

[2]*Center for Integrated Nanotechnologies, Los Alamos National Laboratory, Los Alamos, New Mexico 87545, USA*

[3]*Collaborative Innovation Center of Quantum Matter, Beijing 100190, China*

[4]*Associate Directorate for Chemistry, Life and Earth Sciences, Los Alamos National Laboratory, Los Alamos, New Mexico 87545, USA*

(Received 1 October 2015; revised manuscript received 1 February 2016; published 24 March 2016)

We present a systematic study of both the temperature and frequency dependence of the optical response in TaAs, a material that has recently been realized to host the Weyl semimetal state. Our study reveals that the optical conductivity of TaAs features a narrow Drude response alongside a conspicuous linear dependence on frequency. The weight of the Drude peak decreases upon cooling, following a T^2 temperature dependence, in good agreement with theoretical predictions. Two linear components with distinct slopes dominate the low-temperature optical conductivity. A comparison between our experimental results and theoretical calculations suggests that the linear conductivity below $\sim$230 cm^{-1} arises purely from interband transitions near the Weyl points, providing rich information about the Weyl semimetal state in TaAs.

DOI: 10.1103/PhysRevB.93.121110

Weyl fermions represent a pair of particles with opposite chirality described by the massless solution of the Dirac equation [1]. After a search of more than eight decades for such fermionic fundamental particles in high-energy physics, evidence for their existence remains elusive. Recently, it has been proposed that in a material with two nondegenerate bands crossing at the Fermi level in three-dimensional (3D) momentum space, the low-energy excitations can be described by Weyl equations, allowing a condensed-matter realization of Weyl fermions as quasiparticles [2,3]. The band crossing points are called Weyl points, and materials possessing such Weyl points are thus known as Weyl semimetals (WSMs).

WSMs feature peculiar band structures both in the bulk and on the surface [2,3], leading to novel quantum phenomena that can be probed by both surface- and bulk-sensitive techniques. In the bulk of a WSM, the low-energy excitations are dominated by the Weyl points, where the bands exhibit linear dispersion in all three-momentum directions, producing a 3D analog of graphene. Weyl points can be assigned a chirality and must appear in pairs with opposite chirality. The surface state of a WSM is characterized by Fermi arcs that link the projection of the bulk Weyl points with opposite chiralities in the surface Brillouin zone [2,3]. In addition, WSMs exhibit exotic magnetotransport properties due to the Adler-Bell-Jackiw chiral anomaly [4–7], such as large negative magnetoresistance in the presence of parallel electric (**E**) and magnetic (**B**) fields [5,6].

WSMs only exist in materials where time-reversal symmetry or inversion symmetry is broken [2]. So far, several materials have been theoretically predicted to be WSM candidates, such as the pyrochlore iridates [2,8], $HgCr_2Se_4$ [3], topological insulator heterostructures [9–11], and the solid solutions $ABi_{1-x}Sb_xTe_3$ (A = La or Lu) [12] and $TlBi(S_{1-x}R_x)_2$ (R = Se or Te) [13] in a very narrow doping range close to the topological phase transition. However, due to the requirement of magnetic order that breaks time-reversal symmetry in large domains [2,3,8], complex sample structures [9–11], or extremely precise control of the chemical composition [12,13] in these materials, none of them have been experimentally confirmed to host the WSM state.

Recently, the noncentrosymmetric and nonmagnetic transition-metal monoarsenides/phosphides (TaAs, TaP, NbAs, and NbP) have been predicted to be natural WSMs with 12 pairs of Weyl points [14,15], triggering extensive experimental studies on these materials in search of evidence for the WSM phase [16–25]. Up to date, the presence of Weyl points [17–21], the resulting Fermi arcs in the surface states [16,18–20], and the negative magnetoresistance caused by the chiral anomaly [23,24] have been experimentally observed in these compounds, paving the way for further investigations into WSMs.

Theoretical predictions have indicated that the WSM state also gives rise to intriguing optical responses [9,26,27]. For instance, the real part of the optical conductivity, $\sigma_1(\omega)$, has contributions from both free carriers (leading to a Drude response) and low-energy interband transitions in the vicinity of the Weyl points [27]. The Drude weight in a WSM is expected to vanish as T^2 upon cooling due to a strongly temperature-dependent chemical potential [9,27], while $\sigma_1(\omega)$ associated with interband transitions close to the Weyl points grows linearly with frequency ("ω-linear" conductivity). This ω-linear conductivity has been observed in some Dirac-fermion quasicrystals [28], as well as $ZrTe_5$ [29], a 3D Dirac semimetal [30–33]. Experimentally realizing the above optical properties in the transition-metal monoarsenides/phosphides will provide not only a good test of theoretical predictions, but also important insight into the WSM state in these materials.

In this Rapid Communication, we systematically investigate both the temperature and frequency dependence of the optical response in TaAs. A narrow Drude response and pronounced ω-linear behaviors have been clearly observed in the $\sigma_1(\omega)$ spectra. With decreasing temperature, the Drude

*rpprasan@lanl.gov
†xgqiu@iphy.ac.cn

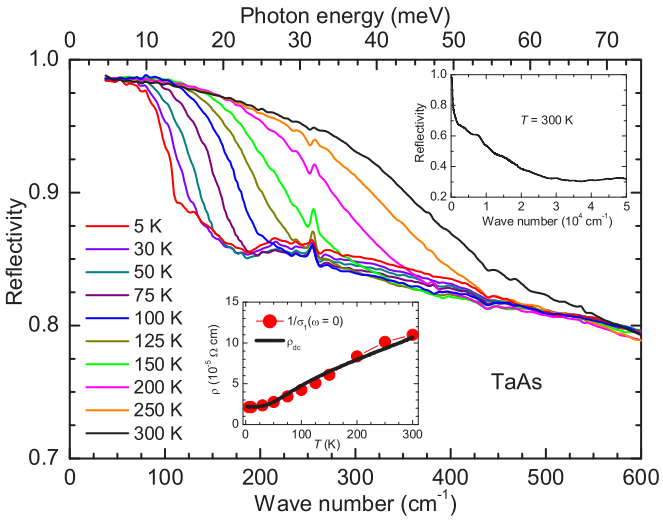

FIG. 1. Far-infrared reflectivity for TaAs at different temperatures. Top inset: 300-K reflectivity over a broad frequency range. Bottom inset: Comparison of the dc resistivity, ρ (solid line), with the zero-frequency values of the Drude fits to the conductivity data (solid circles).

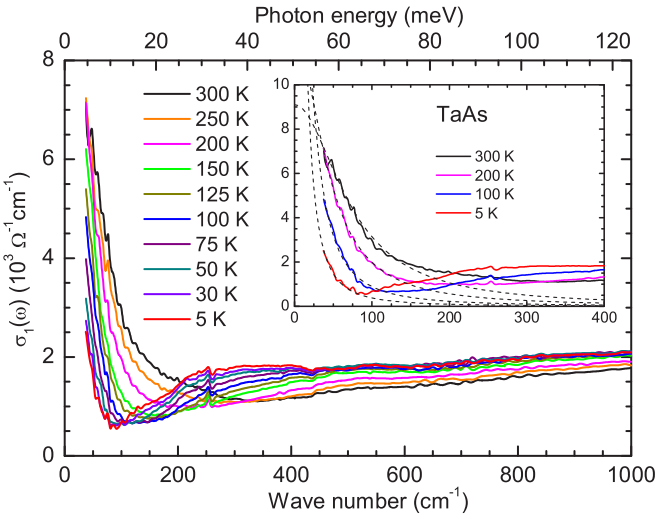

FIG. 2. Temperature-dependent optical conductivity $\sigma_1(\omega)$ in the far-infrared region for TaAs. Inset: Fits to the Drude model (dashed lines) at low frequencies for several representative temperatures.

weight diminishes as T^2, agreeing well with theoretical predictions for a WSM. The low-temperature $\sigma_1(\omega)$ reveals two ω-linear components with distinct slopes. By comparing these observations with first-principles calculations, we find that the ω-linear conductivity below $\sim$230 cm^{-1} originates purely from interband transitions in the vicinity of the Weyl points that are located very close to the Fermi energy. These interband transitions contain rich information about the fundamental properties (such as the chemical potential and Fermi velocity) of the Weyl points in TaAs.

Sample synthesis and characterization, as well as experimental methods and Kramers-Kronig analysis, are described in detail in the Supplemental Material [34].

Figure 1 shows the measured reflectivity [$R(\omega)$] for TaAs in the far-infrared region at different temperatures. The top inset displays the room-temperature $R(\omega)$ up to 50 000 cm^{-1}. The sharp feature at $\sim$250 cm^{-1} is associated with an infrared-active phonon mode [35], which will not be discussed in this Rapid Communication. At 300 K, $R(\omega)$ exhibits a typical metallic response characterized by a well-defined plasma edge below 500 cm^{-1} and a relatively high $R(\omega)$ that approaches unity at zero frequency. The low value of the plasma edge ($<$500 cm^{-1}) generally suggests a very small carrier density [29], consistent with the tiny volumes enclosed by the Fermi surfaces (FSs) in this material [14,15,17,18,23]. As the temperature decreases, the plasma edge shifts continuously towards lower frequencies and becomes steeper, indicating reductions in both the carrier density and scattering rate.

Figure 2 depicts the far-infrared $\sigma_1(\omega)$ of TaAs between 5 and 300 K. At room temperature, the low-frequency $\sigma_1(\omega)$ is dominated by a narrow Drude response, indicating the metallic nature of the material. The width of the Drude peak at half maximum represents the quasiparticle scattering rate, while the area under the Drude peak (spectral weight) is proportional to the free carrier density [36]. As the temperature is reduced, the Drude peak becomes narrower and loses its spectral weight, implying that both the quasiparticle scattering rate and carrier density drop with decreasing temperature. This is consistent with the reflectivity analysis. In addition to the Drude response, a remarkable ω-linear conductivity was observed in the 300-K $\sigma_1(\omega)$ spectrum up to 1000 cm^{-1}. At 5 K, where the Drude peak becomes very small and narrow, another ω-linear component with a different slope emerges in the frequency range $\sim$70–230 cm^{-1}, resulting in a noticeable kink at $\sim$230 cm^{-1} in the 5-K optical conductivity.

We begin with a detailed analysis of the Drude response. In order to quantify the temperature dependence of the Drude peak, at each temperature we fit the low-frequency $\sigma_1(\omega)$ to the well-known Drude model [36],

$$\sigma_1^D(\omega) = \frac{2\pi}{Z_0}\frac{\Omega_{p,D}^2}{\tau_D\left(\omega^2+\tau_D^{-2}\right)}, \tag{1}$$

where $Z_0 \approx 377\Omega$ is the vacuum impedance; $\Omega_{p,D}$ and $1/\tau_D$ correspond to the plasma frequency and scattering rate, respectively. The fitting results are shown as dashed lines in the inset of Fig. 2 for several representative temperatures. The dc resistivity $\rho_{dc} \equiv 1/\sigma_1(\omega = 0)$, derived from the zero-frequency value of the fit curve (solid circles in the lower inset of Fig. 1), agrees very well with transport measurements (solid curve), indicating that our modeling is reliable. The application of the Drude fit at each measured temperature yields the values of $\Omega_{p,D}$ and $1/\tau_D$.

Theoretical calculations have demonstrated that a WSM has a strongly temperature-dependent chemical potential, resulting in a Drude weight that vanishes as T^2 [9,27]. The Drude weight can be easily calculated from $\Omega_{p,D}$,

$$S_{\text{Drude}} = \int_0^\infty \sigma_1^D(\omega)d\omega = \frac{\pi^2}{Z_0}\Omega_{p,D}^2. \tag{2}$$

Figure 3(a) shows the evolution of S_{Drude} with temperature, which follows the T^2 behavior (solid line) quite well, in good agreement with theoretical predictions. Nevertheless, band

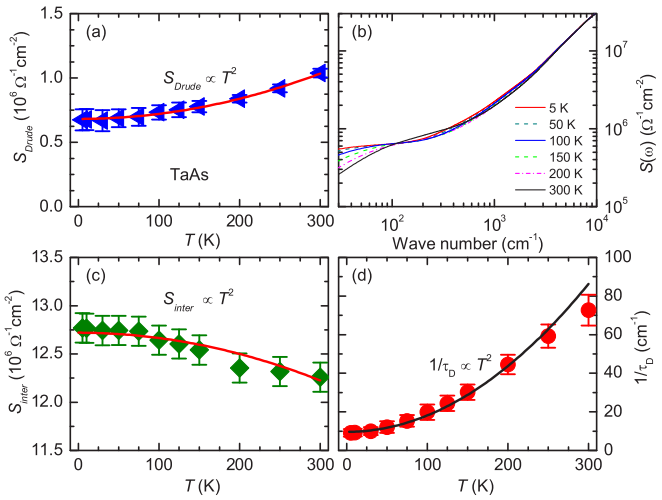

FIG. 3. (a) Temperature dependence of the Drude weight. The solid line is a fit to a parabolic function. (b) Frequency-dependent spectral weight for several representative temperatures. (c) Evolution of the interband spectral weight with temperature. The solid line is a fit to a parabolic function. (d) shows the width of the Drude peak as a function of temperature. The solid line represents a T^2 behavior.

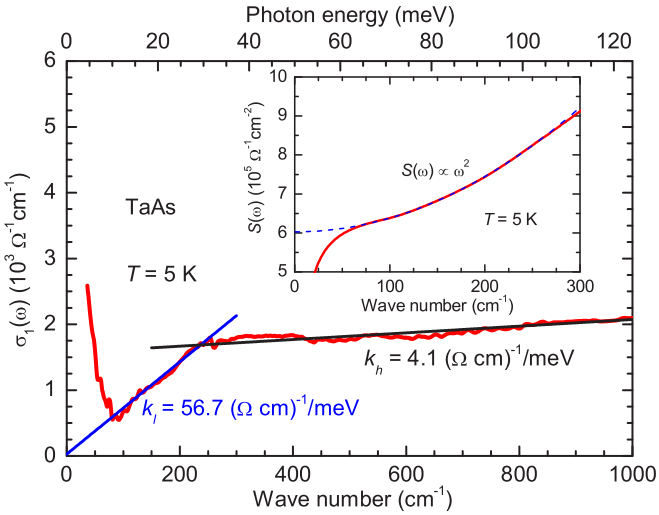

FIG. 4. Optical conductivity for TaAs at 5 K. The blue and black solid lines through the data are linear guides to the eye. The inset shows the spectral weight as a function of frequency at 5 K (red solid curve), which follows an ω^2 behavior (blue dashed line).

structure calculations [14,37] have shown that trivial FSs exist in TaAs, which also contribute to the Drude spectral weight that may vary with temperature.

Theory has further suggested that the missing Drude weight due to the chemical potential shift is transferred to the interband conductivity that lies in a higher frequency range [27]. In order to track the spectral weight transfer, we plot the frequency-dependent spectral weight, defined as $S(\omega) = \int_0^\omega \sigma_1(\omega')d\omega'$, at different temperatures in Fig. 3(b). The $S(\omega)$ curves for all temperatures converge at ~5000 cm^{-1}, indicating that the spectral weight transfer occurs below 5000 cm^{-1} and the missing Drude weight is fully recovered within this energy scale. To further verify the spectral weight transfer, Fig. 3(c) depicts the temperature dependence of the interband spectral weight $S_{\text{inter}} = S_{\text{total}} - S_{\text{Drude}}$, where S_{total} is calculated by integrating $\sigma_1(\omega)$ from 0 to 5000 cm^{-1}. The opposite temperature dependence of S_{inter} and S_{Drude} strongly supports the spectral weight transfer from the Drude response to interband transitions with decreasing temperature.

Figure 3(d) displays $1/\tau_D$ as a function of temperature. It is evident that $1/\tau_D$ decreases as the temperature is lowered, following a T^2 temperature dependence, as shown by the black solid curve through the data points. At low temperatures, $1/\tau_D$ becomes extremely small, in accord with the ultrahigh carrier mobility observed in transport measurements on TaAs [23,24]. Although these properties agree well with the expected behavior for WSMs [26], we would like to point out that a T-quadratic scattering rate, known as Fermi liquid behavior [38], is not unique to WSMs, because this has also been widely observed in topologically trivial materials [38–40].

Having systematically examined the evolution of the Drude response with temperature, we next investigate the $\sigma_1(\omega)$ spectrum associated with interband transitions. Since the Weyl points in TaAs are located in close proximity to the Fermi level [14,15,17,18], they can be obscured by thermal excitations. To avoid this, we focus on the $\sigma_1(\omega)$ spectrum at the lowest measured temperature (5 K). At this temperature, the Drude peak is small and extraordinarily narrow, allowing us to access the low-energy interband transitions near the Weyl points.

Figure 4 shows $\sigma_1(\omega)$ at 5 K up to 1000 cm^{-1}. Two ω-linear components with distinct slopes can be clearly identified in the conductivity spectrum, as indicated by the blue and black solid lines through the data. Both ω-linear components fit well to $\sigma_1(\omega) = \sigma_1(0) + k\omega$, so that their slopes can be directly determined. The slope of the low-energy ω-linear component between 70 and 230 cm^{-1} is $k_l = 56.7$ (Ω cm)$^{-1}$/meV, while the high-energy component between 230 and 1000 cm^{-1} has a slope of $k_h = 4.1$ (Ω cm)$^{-1}$/meV. A linearly increasing $\sigma_1(\omega)$ necessarily leads to a quadratic rise in $S(\omega)$. The inset of Fig. 4 portrays the frequency dependence of $S(\omega)$ at 5 K (red solid line), which precisely follows the expected ω^2 behavior (blue dashed line), confirming that the low-frequency optical response in TaAs is dominated by an ω-linear conductivity at 5 K.

In a noninteracting electron system with two symmetric energy bands touching each other at the Fermi level, $\sigma_1(\omega)$ arising from interband transitions adopts a power-law frequency dependence with $\sigma_1(\omega) \propto (\frac{\hbar\omega}{2})^{(d-2)/z}$, where d and z represent the dimension of the system and the power law of the band dispersion, respectively [41]. This behavior has been experimentally confirmed in two-dimensional graphene ($d = 2$ and $z = 1$) where a frequency-independent optical conductivity was observed [42]. TaAs is a 3D material ($d = 3$). The linear conductivity is therefore a clear signature of linear band dispersion ($z = 1$), which is a hallmark of WSMs.

Further information about the Weyl points in TaAs can be obtained by comparing our optical data with theoretical calculations [26,27], which have demonstrated that the ω-dependent optical conductivity associated with the interband

transitions near the Weyl points is given by

$$\sigma_1(\omega) = \frac{NG_0\omega}{24v_F}\Theta(\omega - 2|\mu|), \quad (3)$$

where N is the number of Weyl points, $G_0 = 2e^2/h = 7.748 \times 10^{-5}\ \Omega^{-1}$ is the quantum conductance, v_F is the Fermi velocity, and μ represents the chemical potential with respect to the Weyl point. This equation indicates that the ω-linear conductivity arising from the Weyl points extrapolates to the origin, regardless of whether or not the Weyl points are on the Fermi surface. This agrees very well with what we observed for the low-energy ω-linear component in TaAs, as shown by the blue solid line in Fig. 4, suggesting its direct link with the Weyl points.

Another deduction from Eq. (3) is that the ω-linear conductivity terminates at $\omega = 2|\mu|$, below which it falls to zero abruptly. In TaAs the low-energy ω-linear component persists down to about 70 cm^{-1} (8.7 meV), below which it overlaps with the Drude peak. This means that $2|\mu| < 8.7$ meV, i.e., the Weyl points that give rise to the low-energy ω-linear component are very close to the Fermi level. First-principles calculations [14,15] have predicted that TaAs possesses 12 pairs of Weyl points in total, and these Weyl points are classified into two types. Four pairs (W1) in the $k_z = 0$ plane are about 2 meV above the Fermi energy, while another eight pairs (W2) off the $k_z = 0$ plane are about 21 meV below the Fermi energy [14]. Therefore, the low-energy ω-linear conductivity we observed here is associated with the low-energy interband transitions close to W1, since the interband transitions close to W2 do not turn on until $\omega > 42$ meV ($\sim$336 cm^{-1}). Moreover, interband transitions involving the trivial bands must be considered with extreme caution. Theoretical calculations have shown that in the presence of spin-orbit coupling, everywhere close to the Fermi level in the bulk Brillouin zone is gapped, with the exception of the 12 pairs of Weyl points [14,15]. Interband transitions involving the trivial bands do not occur below $\sim$30 meV ($\sim$240 cm^{-1}). This suggests that the ω-linear conductivity below 230 cm^{-1} arises purely from the interband transitions in the vicinity of W1.

Equation (3) further implies that the slope of the ω-linear conductivity is directly related to v_F through $k = \frac{NG_0}{24v_F}$. In TaAs, there are four pairs of W1, i.e., $N = 8$. With the slope of the low-energy ω-linear conductivity determined from the linear fit, we can calculate $v_F = 0.286$ eV Å. Both theoretical and experimental studies [17,23] have revealed that W1 is strongly anisotropic, with Fermi velocities of 1.669, 2.835, and 0.273 eV Å along k_x, k_y, and k_z, respectively. Optical conductivity is a momentum-averaged probe, consisting of contributions from all momentum directions. In this sense, the value of v_F derived from our optical data falls into a reasonable range for W1.

We notice that the low-energy ω-linear component exhibits weak humplike features instead of a perfect linearity. Such a behavior may be understood through a close inspection of the band structure. Both theoretical and experimental studies [14,17] have shown that the band dispersion at the Weyl points is indeed not perfectly linear in TaAs. Furthermore, W1 is strongly anisotropic, with a band dispersion varying significantly along different k directions. These effects can reasonably cause weak humplike features in the $\sigma_1(\omega)$ spectrum associated with interband transitions near the Weyl points.

Finally, we discuss the origin of the high-energy ω-linear component (between 230 and 1000 cm^{-1}). The fact that it is linear in ω and turns on at a higher frequency makes it tempting to link this ω-linear component with the eight pairs of Weyl points (W2) lying 21 meV below the Fermi energy. However, as we discussed previously, on this energy scale interband transitions from the trivial bands also set in. In addition, interband transitions associated with W1 still exist. This indicates that the high-energy ω-linear component is a combination of contributions from W1, W2, and the trivial bands. Nevertheless, its robust linearity implies that interband transitions close to the Weyl points may still dominate the frequency dependence of $\sigma_1(\omega)$, since there are 24 Weyl points in total, but only eight trivial bands that contribute to $\sigma_1(\omega)$ in this frequency range. However, if we estimate v_F from $k_h = 4.1\ (\Omega\,\text{cm})^{-1}/\text{meV}$ and $N = 24$, we get $v_F = 11.83$ eV Å. This value does not fall into a reasonable range for any of the Weyl points [17,23], because it is substantially larger than the values along any of the momentum directions for both W1 and W2. These facts suggest that the slope of the high-energy ω-linear component is likely modified by interband transitions from the trivial bands. This may also account for its nonzero intercept.

To summarize, the optical conductivity of TaAs, a recently discovered WSM, has been measured at a variety of temperatures over a broad frequency range. We observed a narrow Drude response alongside ω-linear behaviors in the optical conductivity spectra. A quadratic temperature dependence of the Drude weight was observed, in accordance with theoretical predictions for a WSM. The optical conductivity at 5 K is characterized by two ω-linear components with distinct slopes. The ω-linear component below 230 cm^{-1} arises purely from the interband transitions in proximity to four pairs of Weyl points lying very close to the Fermi energy ($|\mu| < 4.35$ meV), providing important insight into the WSM state in TaAs. In contrast, the linear conductivity above 230 cm^{-1} originates from interband transitions that involve all of the Weyl points as well as the trivial bands. These experimental results thus produce the first verification of theoretical predictions for the optical response of WSMs [9,26,27] in TaAs, setting the stage for further studies in this class of materials.

We acknowledge very illuminating discussions with Simin Nie, Hongming Weng, Yongkang Luo, Hu Miao, John Bowlan, Pamela Bowlan, Brian McFarland, and Ricardo Lobo. Work at IOP CAS was supported by MOST (973 Projects No. 2015CB921303, No. 2015CB921102, No. 2012CB921302, and No. 2012CB821403), and NSFC (Grants No. 91121004, No. 91421304, and No. 11374345). Work at LANL was performed at the Center for Integrated Nanotechnologies, a US Department of Energy, Office of Basic Energy Sciences user facility, and funded by the LANL LDRD program and by the UC Office of the President under the UC Lab Fees Research Program, Grant ID No. 237789. H. Xiao is supported by NSAF, Grant No. U1530402.

B.X. and Y.M.D. contributed equally to this work.

[1] H. Weyl, Z. Phys. **56**, 330 (1929).
[2] X. Wan, A. M. Turner, A. Vishwanath, and S. Y. Savrasov, Phys. Rev. B **83**, 205101 (2011).
[3] G. Xu, H. Weng, Z. Wang, X. Dai, and Z. Fang, Phys. Rev. Lett. **107**, 186806 (2011).
[4] H. Nielsen and M. Ninomiya, Phys. Lett. B **130**, 389 (1983).
[5] D. T. Son and B. Z. Spivak, Phys. Rev. B **88**, 104412 (2013).
[6] P. Hosur and X. Qi, C. R. Phys. **14**, 857 (2013).
[7] S. A. Parameswaran, T. Grover, D. A. Abanin, D. A. Pesin, and A. Vishwanath, Phys. Rev. X **4**, 031035 (2014).
[8] W. Witczak-Krempa and Y. B. Kim, Phys. Rev. B **85**, 045124 (2012).
[9] A. A. Burkov and L. Balents, Phys. Rev. Lett. **107**, 127205 (2011).
[10] G. B. Halász and L. Balents, Phys. Rev. B **85**, 035103 (2012).
[11] A. A. Zyuzin, S. Wu, and A. A. Burkov, Phys. Rev. B **85**, 165110 (2012).
[12] J. Liu and D. Vanderbilt, Phys. Rev. B **90**, 155316 (2014).
[13] B. Singh, A. Sharma, H. Lin, M. Z. Hasan, R. Prasad, and A. Bansil, Phys. Rev. B **86**, 115208 (2012).
[14] H. Weng, C. Fang, Z. Fang, B. A. Bernevig, and X. Dai, Phys. Rev. X **5**, 011029 (2015).
[15] S.-M. Huang, S.-Y. Xu, I. Belopolski, C.-C. Lee, G. Chang, B. Wang, N. Alidoust, G. Bian, M. Neupane, C. Zhang *et al.*, Nat. Commun. **6**, 7373 (2015).
[16] B. Q. Lv, H. M. Weng, B. B. Fu, X. P. Wang, H. Miao, J. Ma, P. Richard, X. C. Huang, L. X. Zhao, G. F. Chen *et al.*, Phys. Rev. X **5**, 031013 (2015).
[17] B. Q. Lv, N. Xu, H. M. Weng, J. Z. Ma, P. Richard, X. C. Huang, L. X. Zhao, G. F. Chen, C. E. Matt, F. Bisti *et al.*, Nat. Phys. **11**, 724 (2015).
[18] S.-Y. Xu, I. Belopolski, N. Alidoust, M. Neupane, G. Bian, C. Zhang, R. Sankar, G. Chang, Z. Yuan, C.-C. Lee *et al.*, Science **349**, 613 (2015).
[19] S.-Y. Xu, N. Alidoust, I. Belopolski, Z. Yuan, G. Bian, T.-R. Chang, H. Zheng, V. N. Strocov, D. S. Sanchez, G. Chang *et al.*, Nat. Phys. **11**, 748 (2015).
[20] L. X. Yang, Z. K. Liu, Y. Sun, H. Peng, H. F. Yang, T. Zhang, B. Zhou, Y. Zhang, Y. F. Guo, M. Rahn *et al.*, Nat. Phys. **11**, 728 (2015).
[21] N. Xu, H. M. Weng, B. Q. Lv, C. Matt, J. Park, F. Bisti, V. N. Strocov, D. Gawryluk, E. Pomjakushina, K. Conder *et al.*, Nat. Commun. **7**, 11006 (2016).
[22] N. J. Ghimire, Y. Luo, M. Neupane, D. J. Williams, E. D. Bauer, and F. Ronning, J. Phys.: Condens. Matter **27**, 152201 (2015).
[23] X. Huang, L. Zhao, Y. Long, P. Wang, D. Chen, Z. Yang, H. Liang, M. Xue, H. Weng, Z. Fang *et al.*, Phys. Rev. X **5**, 031023 (2015).
[24] C.-L. Zhang, S.-Y. Xu, I. Belopolski, Z. Yuan, Z. Lin, B. Tong, G. Bian, N. Alidoust, C.-C. Lee, S.-M. Huang *et al.*, Nat. Commun. **7**, 10735 (2016).
[25] Y. Luo, N. J. Ghimire, M. Wartenbe, H. Choi, M. Neupane, R. D. McDonald, E. D. Bauer, J. Zhu, J. D. Thompson, and F. Ronning, Phys. Rev. B **92**, 205134 (2015).
[26] P. Hosur, S. A. Parameswaran, and A. Vishwanath, Phys. Rev. Lett. **108**, 046602 (2012).
[27] P. E. C. Ashby and J. P. Carbotte, Phys. Rev. B **89**, 245121 (2014).
[28] T. Timusk, J. P. Carbotte, C. C. Homes, D. N. Basov, and S. G. Sharapov, Phys. Rev. B **87**, 235121 (2013).
[29] R. Y. Chen, S. J. Zhang, J. A. Schneeloch, C. Zhang, Q. Li, G. D. Gu, and N. L. Wang, Phys. Rev. B **92**, 075107 (2015).
[30] Q. Li, D. E. Kharzeev, C. Zhang, Y. Huang, I. Pletikosić, A. V. Fedorov, R. D. Zhong, J. A. Schneeloch, G. D. Gu, and T. Valla, Nat. Phys. (2016).
[31] H. Weng, X. Dai, and Z. Fang, Phys. Rev. X **4**, 011002 (2014).
[32] Z. Wang, Y. Sun, X.-Q. Chen, C. Franchini, G. Xu, H. Weng, X. Dai, and Z. Fang, Phys. Rev. B **85**, 195320 (2012).
[33] Z. Wang, H. Weng, Q. Wu, X. Dai, and Z. Fang, Phys. Rev. B **88**, 125427 (2013).
[34] See Supplemental Material at http://link.aps.org/supplemental/10.1103/PhysRevB.93.121110 for sample synthesis and characterization, as well as experimental methods and Kramers-Kronig analysis.
[35] H. W. Liu, P. Richard, Z. D. Song, L. X. Zhao, Z. Fang, G.-F. Chen, and H. Ding, Phys. Rev. B **92**, 064302 (2015).
[36] M. Dressel and G. Grüner, *Electrodynamics of Solids* (Cambridge University Press, Cambridge, UK, 2002).
[37] C.-C. Lee, S.-Y. Xu, S.-M. Huang, D. S. Sanchez, I. Belopolski, G. Chang, G. Bian, N. Alidoust, H. Zheng, M. Neupane *et al.*, Phys. Rev. B **92**, 235104 (2015).
[38] H. v. Löhneysen, A. Rosch, M. Vojta, and P. Wölfle, Rev. Mod. Phys. **79**, 1015 (2007).
[39] K. Jin, N. P. Butch, K. Kirshenbaum, J. Paglione, and R. L. Greene, Nature (London) **476**, 73 (2011).
[40] Y. M. Dai, H. Miao, L. Y. Xing, X. C. Wang, P. S. Wang, H. Xiao, T. Qian, P. Richard, X. G. Qiu, W. Yu *et al.*, Phys. Rev. X **5**, 031035 (2015).
[41] A. Bácsi and A. Virosztek, Phys. Rev. B **87**, 125425 (2013).
[42] K. F. Mak, M. Y. Sfeir, Y. Wu, C. H. Lui, J. A. Misewich, and T. F. Heinz, Phys. Rev. Lett. **101**, 196405 (2008).